

## Corrosion Inhibition of N80 Steel with the Presence of Asymmetric Gemini in a CO<sub>2</sub>-saturated Brine Solution

Hu Wang<sup>1</sup>, Jun Tang<sup>1</sup>, Juan Xie<sup>1,2,\*</sup>

<sup>1</sup> School of Materials Science and Engineering, Southwest Petroleum University, Chengdu 610500, China

<sup>2</sup> School of Chemistry and Chemical Engineering, Southwest Petroleum University, Chengdu 610500, China

\*E-mail: [Jennyx99@126.com](mailto:Jennyx99@126.com)

Received: 7 June 2017 / Accepted: 7 July 2017 / Published: 12 October 2017

---

Corrosion inhibition effects of asymmetric gemini corrosion inhibitor on N80 steel in a CO<sub>2</sub>-saturated brine solution had been investigated by weight loss and electrochemical measurements. The synergistic effects of gemini with thiourea (TU), thiazole (TZ) and pyridine (PD) were also studied with weight loss and electrochemical measurements. The results revealed that asymmetric gemini corrosion inhibitor displayed excellent corrosion inhibition performance at 70°C in CO<sub>2</sub>-saturated brine solution. The inhibitor was anodic type in nature. There existed apparent synergistic effect between asymmetric gemini inhibitor and other ingredients. The mixture inhibitors can provide excellent protection to N80 steel at test condition. The best formula of mixture inhibitors was then presented. The synergistic mechanism of gemini with other ingredients were also discussed.

---

**Keywords:** N80 steel, gemini corrosion inhibitor, synergistic effect, weight loss, electrochemical measurement

### 1. INTRODUCTION

As one of the most important countermeasures to corrosion of metals, adding corrosion inhibitor has been intensively applied in industry [1-4]. Especially in petroleum and natural gas exploitation, all kinds of commercial corrosion inhibitors are used to guarantee the production. Quaternary ammonium salt is a commonly used type, including imidazoline quaternary ammonium salt. Imidazoline, which has nitrogen containing ring in chemical structure and been regarded as excellent electron donor, is the most widely used corrosion inhibitor in application [5-7]. Although the

commonly used imidazoline inhibitor has very excellent inhibition efficiency, the relatively high dosage and expensive in raw materials have hindered its further development in application [8-10].

Hence, the use of mixture corrosion inhibitor in industrial applications is more common than one ingredient corrosion inhibitor. Thousands of commercial corrosion inhibitors with mixture ingredients have been exploited. The synergistic effects between chemicals as corrosion inhibitor have also been carried out as research work in lab. However, the research work about synergistic effects is far more lagged by the application of mixture inhibitor in industry. More research work should be done to elucidate the synergism and, also, to guide the formulation of mixture corrosion inhibitor.

The synergistic effects of imidazoline inhibitor with other ingredients in preventing corrosion of metals have been investigated in recent years. Jingmao Zhao et al. [11] studied the synergistic effects on mild steel surface with the presence of imidazoline and sodium benzoate in saturated CO<sub>2</sub> solution. It was shown that sodium benzoate remarkably enhanced the inhibition efficiency of imidazoline. There were obvious synergism between imidazoline and sodium benzoate. The adsorption process was also proposed by a model to explain the synergism mechanism. P. C. Okafor et al. [12] found that apparent synergistic effect existed between imidazoline salt (2M2) and thiourea (TU) on N80 steel surface in NaCl solutions with saturated CO<sub>2</sub>. It is shown that the 2M2 can steady TU molecules at the interface. The compounds inhibit the corrosion reactions via their polycentric adsorption sites on metal surface. The action of 2M2 obeys Langmuir adsorption isotherm. More synergism studies between imidazolines and halides had been extensively reported [13-17].

Gemini surfactants have been popular in recent years. The use of gemini surfactant as corrosion inhibitor has been reported extensively [18-23]. Gemini surfactant is commonly consisted of two hydrophilic groups and two hydrophobic groups in structure. It is reported that this kind of surfactant is more liable to form micelles in solution than conventional surfactants, which indicates better solubility and greater efficiency in lowering the surface tension. In addition, the two hydrophilic groups enhance the adsorption on metal surface and two hydrophobic groups can form a better barrier to water.

In this paper, the performance of asymmetric gemini inhibitor in inhibiting corrosion of N80 steel had been studied in a CO<sub>2</sub>-saturated brine solution at 70°C by weight loss and electrochemical measurements. In addition, the synergistic effects of asymmetric gemini inhibitor with TU, thiazole (TZ) and pyradine (PD) were also performed with weight loss and electrochemical measurements.

## 2. EXPERIMENTAL

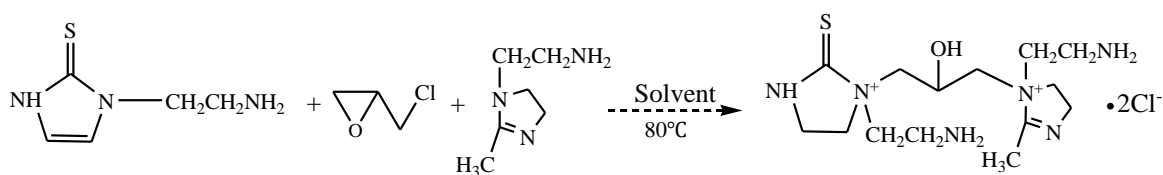


**Figure 1.** The synthetic reaction and chemical structures of the gemini inhibitor.

The asymmetric gemini inhibitor was synthesized as expressed in Fig.1 and purified in lab. The brine solution was composed of 1.265 g/L CaCl<sub>2</sub>, 0.148 g/L Na<sub>2</sub>SO<sub>4</sub>, 2.896 g/L NaCl, 0.556 g/L KCl,

1.309 g/L  $\text{MgCl}_2 \cdot 6\text{H}_2\text{O}$ , 0.497 g/L  $\text{NaHCO}_3$  and 0.056 g/L  $\text{NaCO}_3$ , which is from the produced water in an offshore oilfield in China. And all the reagents used in the experiments, including thiourea (TU), thiazole (TZ) and pyridine (PD), were purchased from Aladdin Industrial Corporation and are all analytical grades. The experiments were carried out at  $70^\circ\text{C}$ , which is the temperature of production system.

N80 steel was used as experimental material with the chemical composition (wt) of C (0.395%), Si (0.242%), Mn (1.400%), P (0.017%), S (0.004%), Cr (0.063%), Ni (0.071%), Mo (0.025%), Cu (0.114%), V (0.110%) and Fe (remainder). The specimens used in all weight loss experiments were sheets of  $40\text{ mm} \times 10\text{ mm} \times 2\text{ mm}$ . In electrochemical experiments, the rectangular specimens were embedded with epoxy resin, leaving an area of  $10\text{ mm} \times 10\text{ mm}$  exposed to the electrolyte. All specimens were abraded gradually with silicon carbide paper from 800 up to 2000 grits, washed with de-ionized water, ethanol, acetone, and dried in cold air before experiments.

In weight loss measurements, the specimens were soaked in the test solution for 72 hours in a static condition. The solution was deaerated and saturated with  $\text{CO}_2$  beforehand. After the experiment, The corrosion products upon the specimen surface were removed by pickling solution with inhibitor (10% HCl + 1% hexamethylenetetramine, soaking in room temperature for 3 minutes) after taking out from static weight loss experiments. Then the specimens were cleaned, dried and weighed for calculating the corrosion rate. The corrosion rate was calculated according to the following equation:

$$r = \frac{W_1 - W_0}{S \times t} \quad (1)$$

where  $r$  represents the corrosion rate in weight loss experiment.  $W_0$  and  $W_1$  are the weighed mass before and after experiment.  $S$  stands for exposed surface area. And  $t$  is the experiment time, 72 hours.

The corrosion inhibition efficiency can be calculated according to the following expression:

$$\eta = \frac{r_0 - r}{r_0} \times 100\% \quad (2)$$

where  $\eta$  represents the corrosion inhibition efficiency.  $r_0$  and  $r$  are the corrosion rates in the absence and presence of the corrosion inhibitor, respectively. Three specimens were used in each measurement.

In high temperature and pressure experiment, an autoclave was used to evaluate the corrosion performance (FCX-2, Dalian Kema Instrument Co. Ltd.). Three N80 specimens were fastened on the holder in the autoclave. Solution used here was the similar with the static experiment. In order to mimic the production atmosphere, 2 hours pumping of nitrogen gas and then 2 hours carbon dioxide were carried out before experiment. The experiment time was 72 hours. The total pressure and partial pressure of  $\text{CO}_2$  in the experiment were 1.5MPa and 0.5MPa, respectively, which were the actual pressures in production. The flow rate, calculated from angular velocity, was set at 1.5 m/s. The temperature was also set at  $70^\circ\text{C}$ .

The electrochemical measurements were conducted by Iviumstat Electrochemical Interface (Ivium Technologies, Netherlands). The electrochemical cell was filled with 250 ml of solution. The solution was degassed and saturated with  $\text{CO}_2$  before test. Saturated calomel electrode (SCE) and platinum bar were used as the reference electrode and counter electrode, respectively. The working electrode, N80 steel, was soaked in the test solution for 0.5 h before test. The scanning range of

polarization curve measurement was from -0.250 V (vs. open circuit potential, OCP) to +0.250 V (vs. OCP) with a scanning rate of 0.3 mV/s. The corresponding parameters can be obtained by fitting the curve. The corrosion inhibition efficiency can also be obtained by the following equation:

$$\eta = \frac{I_{\text{corr}(0)} - I_{\text{corr}(1)}}{I_{\text{corr}(0)}} \times 100\% \quad (3)$$

where  $\eta$  represents the corrosion inhibition efficiency.  $I_{\text{corr}(0)}$  and  $I_{\text{corr}(1)}$  stand for corrosion current densities without and with corrosion inhibitor. In electrochemical impedance spectroscopy measurement (EIS), the amplitude of the applied alternative current was  $\pm 10$  mV. All the EIS tests were under OCP. The frequency ranged from  $10^5$  Hz to  $10^{-2}$  Hz. In EIS measurement, the inhibition efficiency can be interpreted as the following equation:

$$\eta = \frac{R_p' - R_p}{R_p} \times 100\% \quad (4)$$

where  $\eta$  represents the corrosion inhibition efficiency,  $R_p'$  and  $R_p$  stand for the charge transfer resistance without and with inhibitor, respectively.

The surface morphologies with different corrosion inhibitor addition conditions were compared by scanning electronic microscopy (SEM, EVO MA 15, Zeiss Nano Techno.). All the SEM pictures were from the weight loss experiments.

### 3. RESULTS AND DISCUSSION

#### 3.1 Inhibition behavior of gemini corrosion inhibitor by weight loss measurement

Fig. 2 shows the influence of concentration of gemini corrosion inhibitor on corrosion rate and inhibition efficiency of N80 steel in brine solution with saturated  $\text{CO}_2$ . It demonstrates that with the rise of inhibitor concentration, the corrosion rate sharply decreases and the inhibition efficiency goes up gradually, reaching maximum value of 83.2% at the concentration of 80 mg/L. The result implies that the gemini corrosion inhibitor is effective in inhibiting corrosion process of N80 steel in near neutral solution. The results are identical with reports in references [24-26].

Many adsorption models had been tried to fit the adsorption behavior of gemini corrosion inhibitor in brine solution. The result shows the Langmuir adsorption fits the best, as is shown in Fig.3. The linear fitting of Langmuir adsorption reveals that regression coefficients are more than 0.99, implying that the adsorption fits Langmuir adsorption well [27]. The equation of Langmuir adsorption can be expressed as follows [28]:

$$\frac{C_{\text{inh}}}{\theta} = \frac{1}{K} + C_{\text{inh}} \quad (5)$$

$$K = \frac{1}{55.5} \exp\left(-\frac{\Delta G_{\text{ads}}^0}{RT}\right) \quad (6)$$

where  $C_{\text{inh}}$  stands for the inhibitor concentration,  $\theta$  is the surface coverage,  $K$  represents the adsorptive equilibrium constant,  $\Delta G_{\text{ads}}^0$  is on behave of the standard free energy of adsorption,  $R$  is the gas constant and  $T$  is the absolute temperature [29, 30]. The calculated free energy of adsorption,  $\Delta G_{\text{ads}}^0$ , is  $-26.2 \text{ kJ mol}^{-1}$ . It is shown that all the  $\Delta G_{\text{ads}}^0$  values are negative, indicating the adsorption process of inhibitor on N80 surface are spontaneous process. It is also universally regarded that the

adsorption mechanism can be judged by free energy  $\Delta G_{ads}^0$ , where  $\Delta G_{ads}^0$  values up to  $-20\text{kJ/mol}$  are regarded as the electrostatic interaction between charged molecules and charged metal surface (physisorption). While if  $\Delta G_{ads}^0$  values are less than  $-40\text{kJ/mol}$ , it is considered as charge sharing or transfer from the inhibitor molecules to the metal surface to form a coordinate covalent bond (chemisorption) [3, 31]. In our study, the  $\Delta G_{ads}^0$  value is between  $-20\text{kJ/mol}$  and  $-40\text{kJ/mol}$ , which implies the adsorption is neither typical physisorption nor typical chemisorption, but a complex mixed type.

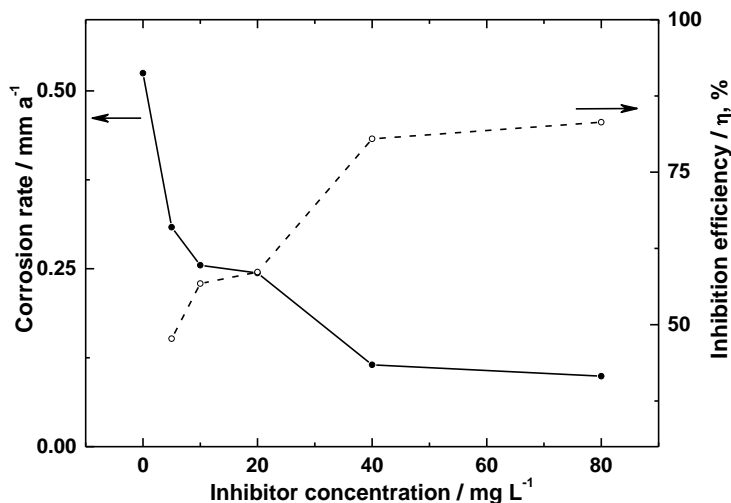


**Figure 2.** Influence of inhibitor concentration on corrosion rate and inhibition efficiency of N80 steel in simulated brine solution at 70°C by weight loss experiments for 72 hours.

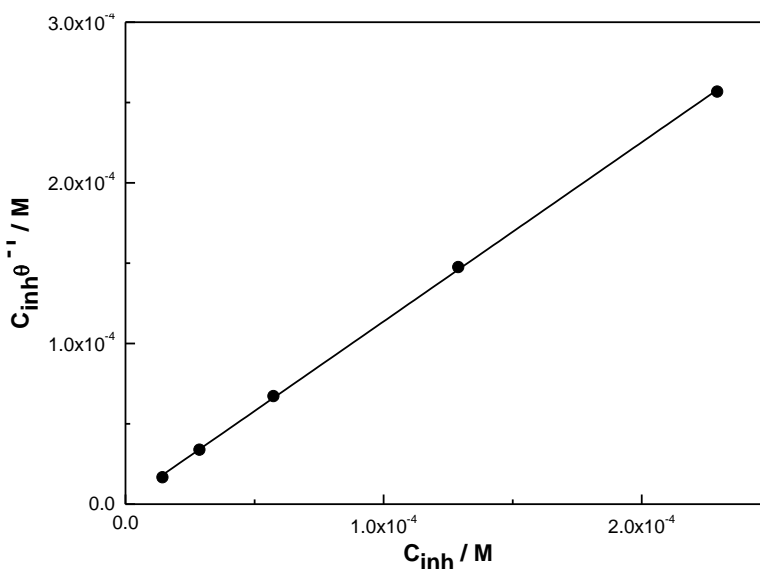


**Figure 3.** Fitting of experimental data from Fig. 2 by Langmuir adsorption.

### 3.2 Electrochemical behavior of gemini corrosion inhibitor in CO<sub>2</sub>-saturated brine solution.

Fig. 4 shows the potentiodynamic polarization curves of N80 steels in CO<sub>2</sub>-saturated solution with different gemini concentrations at 70°C. Table 1 is the corresponding electrochemical parameters fitted from Fig. 4. It is shown that the shapes of all the polarization curves are almost the same, which

indicates that the corrosion mechanism, both anodic and cathodic, have not been changed with the addition and concentration of the gemini corrosion inhibitor. The anodic process, which is in direct relation with corrosion event, is apparently an active dissolution of steel in all condition [32]. Although the shapes of polarization curves in all conditions are similar, the positions of curves in plane-coordinate system are different. With the presence of corrosion inhibitor, the curves move to the upper left of the plane-coordinate system. Furthermore, with the increase of concentration, the shifting amount of the curve gradually increases. Table 1 also proves the behavior presented in Fig. 4. With the presence and concentration increase of gemini corrosion inhibitor,  $E_{\text{corr}}$  (corrosion potential) moves positively gradually, implying that the anodic process is more apparently influenced by the addition of gemini corrosion inhibitor, although the largest shifting of  $E_{\text{corr}}$  is only 59 mV [31]. It is generally believed that the inhibitor can be regarded as cathodic or anodic type when the shifting of corrosion potential is more than 85mV [33]. Hence, the mechanism of gemini inhibitor is mixed type in nature. Meantime, the cathodic ( $b_c$ ) and anodic ( $b_a$ ) Tafel slopes remarkably decrease with the adding of gemini corrosion inhibitor. While, the behavior of inhibitor concentration on  $b_a$  and  $b_c$  is not very clear. All above behaviors reveal that the gemini inhibitor is a mixed-type corrosion inhibitor in nature, in which both cathodic and anodic processes have been inhibited by the adsorption of gemini inhibitor [34]. As a result, the corrosion current density,  $I_{\text{corr}}$ , decreases with the adding of corrosion inhibitor. Additionally, with the increase of inhibitor concentration,  $I_{\text{corr}}$  keeps declining and inhibition efficiency,  $\eta$ , gradually rises and reaches the peak of 88.2% at 80 mg/L. It is evidently proved that gemini corrosion inhibitor is very effective in inhibiting corrosion of N80 steel in brine solution with saturated  $\text{CO}_2$ .

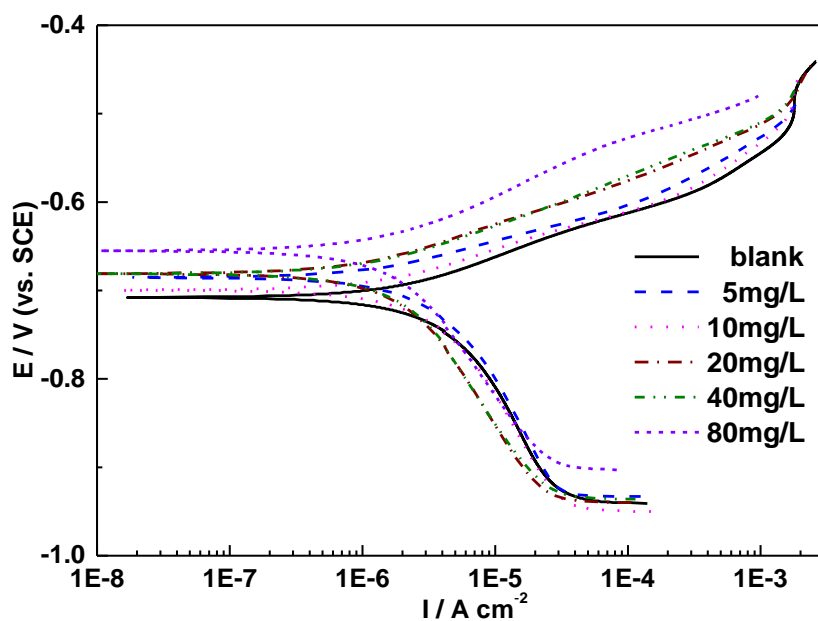


**Figure 4.** Potentiodynamic polarization curves of N80 steel in near neutral solution with different concentrations of gemini inhibitor at 70°C.

**Table 1.** Electrochemical parameters from polarization curves of N80 steel in the absence and presence of three gemini inhibitors in a CO<sub>2</sub>-saturated brine solution at 70°C

Conc. / mgL <sup>-1</sup>	E <sub>corr</sub> / V	I <sub>cor</sub> /10 <sup>-7</sup> A cm <sup>-2</sup>	b <sub>a</sub> / mV dec <sup>-1</sup>	-b <sub>c</sub> / mV dec <sup>-1</sup>	η / %
blank	-0.704	98.5	192	1201	-
5	-0.651	18.9	78	140	80.8
10	-0.670	20.5	79	154	79.2
20	-0.681	31.5	89	209	68.0
40	-0.681	29.4	82	228	70.1
80	-0.655	11.6	74	146	88.2

EIS measurements also demonstrate that the asymmetric gemini inhibitor behave excellent inhibiting property to the corrosion of N80 steel in brine solution containing saturated CO<sub>2</sub>. Fig. 5 displays the influence of the inhibitor addition on EIS. It can be observed in Nyquist plot that in the presence of inhibitor, the magnitude of the impedance sharply increases by contrast with the absence of inhibitor. Furthermore, the semi-circle of impedance is continuously enlarged with the rise of concentration. It reveals the gemini corrosion inhibitor can provide efficient protection to via film forming at interface [35-37]. Furthermore, with the increase of the magnitude of impedance, the inhibition performance will be enhanced. The inhibition efficiency can also be calculated from the impedance, R<sub>ct</sub>. Bode plots demonstrate similar mechanism for different concentrations of corrosion inhibitor. Electrochemical parameters obtained from fitting of EIS plots by equivalent circuit are shown in Table 2. n, phase shift, is always around 0.73, implying it is influenced by the charge transfer and the inhomogeneities, like roughness at metal surface [38]. This also can be figured out by the depressed capacitive semicircular at Nyquist plots. The inhibition efficiency, η, is quite high in all tested inhibitor concentration, more than 90%. It is further proved the inhibitor displays excellent film forming ability.

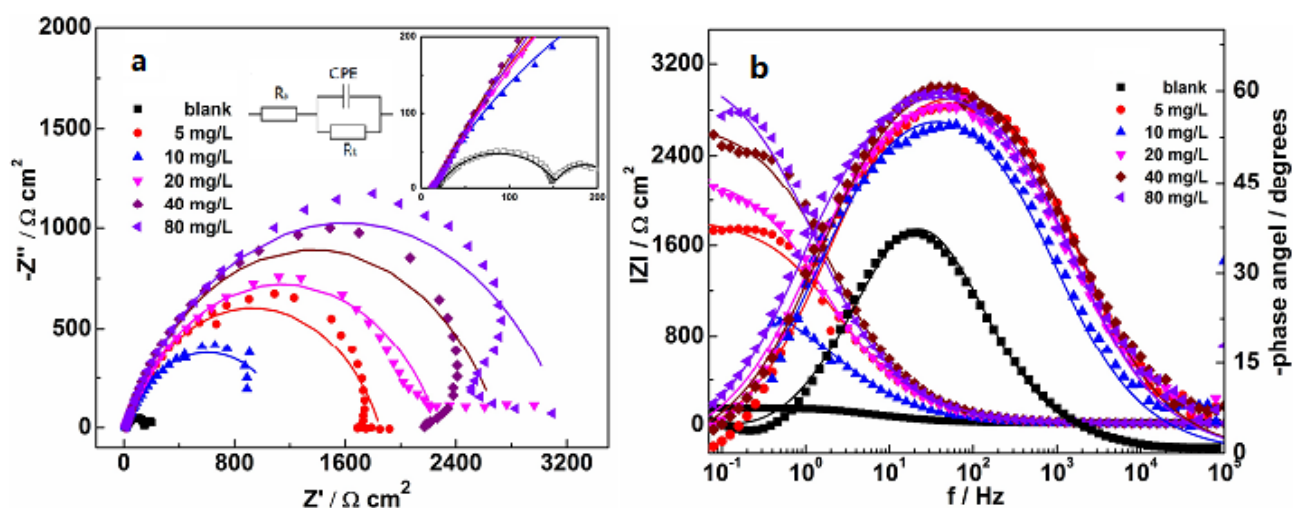


**Figure 5.** EIS plots, Nyquist plot (a) and Bode plot (b), of N80 steel in a CO<sub>2</sub>-saturated brine solution at 70°C with different additions of asymmetric gemini inhibitor.

**Table 2.** Electrochemical parameters obtained from fitting with the model of equivalent circuit for all experimental data in Fig.5.

Concentration / mg L <sup>-1</sup>	R <sub>ct</sub> / Ω cm <sup>2</sup>	CPE / μΩ <sup>-1</sup> s <sup>n</sup> cm <sup>2</sup>	n	η / %
0	62	469	0.74	-
5	1839	91	0.74	96.6
10	1186	165	0.72	94.8
20	2261	101	0.72	97.3
40	2701	71	0.74	97.7
80	3184	88	0.73	98.1

### 3.3 Use of mixture corrosion inhibitor and synergist effects between asymmetric gemini and other inhibitors.

In practical use of corrosion inhibitor, the mixtures of different kinds of inhibitors are commonly applied. The use of mixture corrosion inhibitor is on the basis of economic consideration. Although the mixture corrosion inhibitors are widely used in industrial applications, the research work on mechanism of synergism within chemicals are still limited and lagged behind. Herein, several commonly used corrosion inhibitors, thiourea, thiazole and pyridine, were used to compound with asymmetric gemini as mixture corrosion inhibitors. It is shown that in blank solution (without corrosion inhibitor), the corrosion rate in static is even higher than in autoclave. It can be ascribed to the formation of corrosion products at N80 surface at high pressure [39]. The presence of different mixture inhibitors manifests different synergistic effects. In comparison with 20 mg/L gemini inhibitor alone, all mixture inhibitors display enhanced inhibition efficiency, indicating apparent synergistic effects occur. Additionally, mixture of 10 mg/L gemini + 2 mg/L TU + 5 mg/L TZ + 5 mg/L PD exhibits the best inhibition performance in all, no matter in static or autoclave conditions.

**Table 3.** Weight loss results of mixture corrosion inhibitors in static and autoclave experiments of N80 steel at 70°C for 72 hours.

Experiments	Inhibitor Addition	Corrosion rate / mm a <sup>-1</sup>	η / %
Static	blank	0.5249	-
Autoclave	blank	0.4773	0
Static	20 mg/L gemini	0.2439	58.6
	10 mg/L gemini + 2 mg/L TU	0.1671	71.7
	10 mg/L gemini + 2 mg/L TU + 5 mg/L TZ + 5 mg/L PD	0.0644	89.1
Autoclave	20 mg/L gemini	0.1540	67.7
	10 mg/L gemini + 2 mg/L TU	0.0932	80.5
	10 mg/L gemini + 2 mg/L TU + 5 mg/L TZ + 5 mg/L PD	0.0272	94.3

Polarization curves in the absence and presence of different formulated gemini corrosion inhibitors are presented in Fig. 6. It can be seen from the figure that the presence of all inhibitors induces notable shifting of the polarization curve. All the curves with addition of inhibitors move to the upper left of the plane-coordinate system, indicating the film forming of inhibitors influences the anodic process of corrosion more than the cathodic one [40]. The corresponding electrochemical parameters illustrate that the absolute values of both  $b_a$  and  $b_c$  decrease with the adding of each inhibitor. Especially in mixture inhibitor of 10 mg/L gemini + 2 mg/L TU + 5 mg/L TZ + 5 mg/L PD, the anodic Tafel slope remarkably decreases to 74 mV dec<sup>-1</sup>, which indicates the anodic process is preferentially inhibited than cathodic one. The  $E_{corr}$  of this mixture inhibitor also displays the largest shifting towards positive direction. Moreover, the corrosion current density,  $I_{corr}$ , of this mixture reaches  $4.80 \times 10^{-7}$  A cm<sup>-2</sup>. All the results denote that the above mixture inhibitor can provide excellent protection to N80 steel in the tested solution by inhibiting the anodic process of corrosion process mainly.

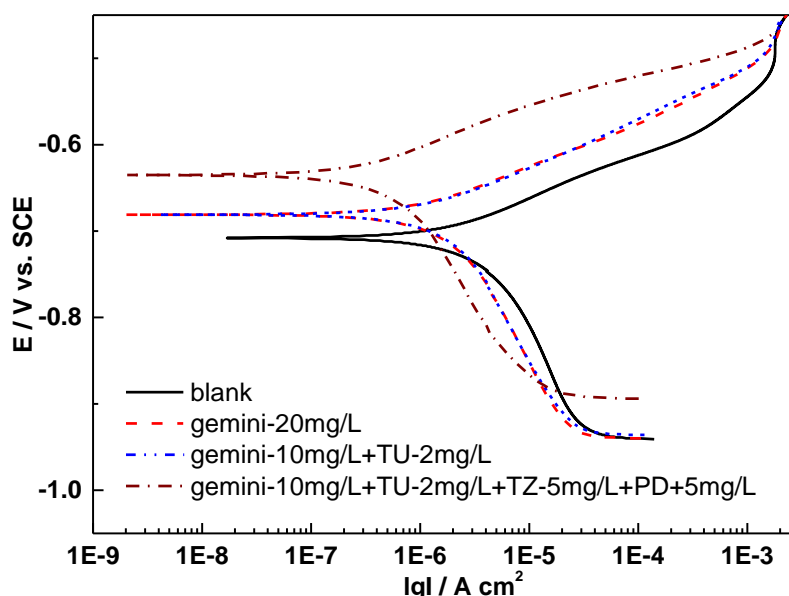


**Figure 6.** Polarization curves of different addition of corrosion inhibitors in a CO<sub>2</sub> saturated brine solution at 70°C.

**Table 4.** Electrochemical parameters fitted from polarization curves of Fig. 6.

Concentration	$E_{corr}/V$	$I_{cor} / 10^{-7} \text{ A cm}^{-2}$	$b_a / \text{mV dec}^{-1}$	$-b_c / \text{mV dec}^{-1}$	$\eta / \%$
blank	-0.7042	98.5	192	1201	-
20 mg/L gemini	-0.6813	31.5	249	209	68.0
10 mg/L gemini + 2 mg/L TU	-0.6803	24.6	255	204	75.0
10 mg/L gemini + 2 mg/L TU + 5 mg/L TZ + 5 mg/L PD	-0.5949	4.80	74	223	95.1

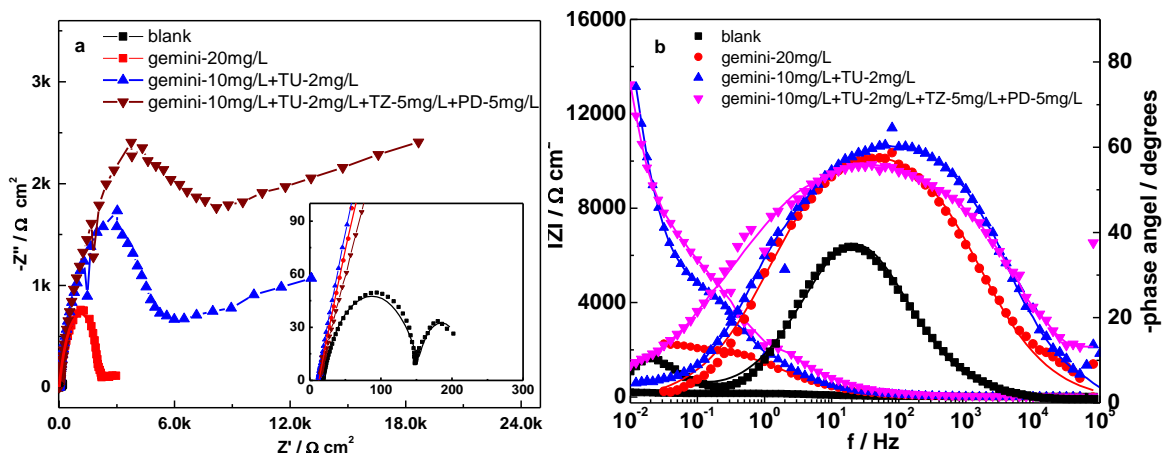


**Figure 7.** EIS plots (a Nyquist plots and b Bode plots) of different corrosion inhibitors in a CO<sub>2</sub> saturated brine solution at 70°C

**Table 5.** Electrochemical parameters obtained from fitting of EIS plots of Fig. 7.

Inhibitors	CPE / $10^{-6} \text{ s}^n \Omega^{-1} \text{ cm}^{-2}$	n	R <sub>ct</sub> / $\Omega \text{ cm}^2$	W / $10^{-4} \Omega \text{ cm}^2$	$\eta$ / %
blank	469	0.78	62	-	-
20 mg/L gemini	101	0.72	2261	-	97.3
10 mg/L gemini + 2 mg/L TU	57.9	0.73	6048	12.8	99.0
10 mg/L gemini + 2 mg/L TU + 5 mg/L TZ + 5 mg/L PD	60.4	0.66	10560	10.8	99.4

EIS plots, shown in Fig. 7, exhibit different patterns for mixture inhibitors by comparing with blank solution and presence of gemini inhibitor only. In EIS plots of mixture inhibitors, Warburg impedance emerges at low frequency, which means the corrosion process is controlled by diffusing [41]. In other words, the compound film at metal surface presents better protection than adding gemini inhibitor only. The charge transfer resistance, R<sub>ct</sub>, represents the inhibition property of adsorption film of inhibitor, which implies the higher the R<sub>ct</sub> value is, the better the inhibition performance will be [42]. The impedance of R<sub>ct</sub> rockets to 10560 Ω cm<sup>2</sup> in mixture inhibitor of 10 mg/L gemini + 2 mg/L TU + 5 mg/L TZ + 5 mg/L PD, which is much bigger than the blank value of 62 Ω cm<sup>2</sup>. Also, the inhibition efficiency reaches to the peak of 99.4% in all solutions. All above results show that the mixture inhibitors exhibit better inhibition efficiency than gemini alone. There exists apparent synergistic effect between the inhibitors. The mixture inhibitor of 10 mg/L gemini + 2 mg/L TU + 5 mg/L TZ + 5 mg/L PD exhibits the best performance in inhibiting corrosion of N80 steel.

### 3.4 SEM morphologies.

Surface morphologies of different conditions of weight loss experiments were presented in Fig. 8 reveals that as the addition of corrosion inhibitor, the N80 surface gets well protected. In blank

solution, the metal surface had been seriously corroded, as shown in Fig. 8a. The presence of 20mg/L gemini inhibitor can apparently but partly protect the surface away from corrosion attack. Mixture inhibitor of 10 mg/L gemini + 2 mg/L TU is better but some small pitting can be spotted.

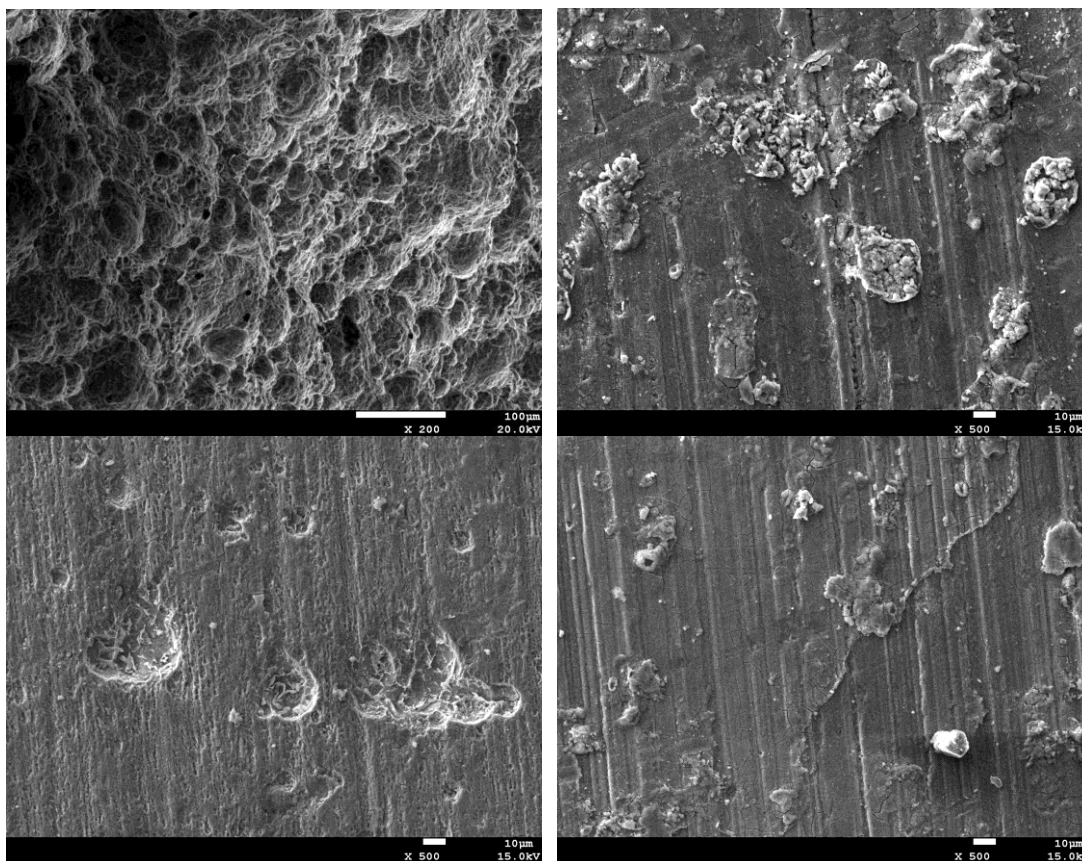


**Figure 8.** Surface morphologies of SEM from previous weight loss experiments: a) N80 steel in the blank solution; b) N80 steel with 20mg/L gemini inhibitor; c) N80 steel with 10 mg/L gemini + 2 mg/L TU; d) N80 steel with 10 mg/L gemini + 2 mg/L TU + 5 mg/L TZ + 5 mg/L PD

The mixture inhibitor of 10 mg/L gemini + 2 mg/L TU + 5 mg/L TZ + 5 mg/L PD can provide the best protection, as shown in Fig. 8d. The N80 surface is quite smooth and intact.

#### 4. CONCLUSIONS

(1) Weight loss, potentiodynamic polarization curves and EIS measurements prove that the asymmetric gemini corrosion inhibitor displays excellent inhibition performance in brine solution with saturated CO<sub>2</sub> at 70°C.

(2) The gemini corrosion inhibitor adsorbs on N80 surface via Langmuir adsorption model. The value of free energy ( $\Delta G_{ads}^0$ ) of adsorption for gemini inhibitor is -26.2 kJ mol<sup>-1</sup>, indicating a mixed type, both chemisorption and physisorption.

(3) Polarization curves indicate that the gemini inhibitor is anodic corrosion inhibitor by

inhibiting anodic dissolution process.

(4) There exists apparent synergistic effect between gemini and other inhibitors. The mixture inhibitors provide excellent protection to N80 steel. The best formula of mixture inhibitors is 10 mg/L gemini + 2 mg/L TU + 5 mg/L TZ + 5 mg/L PD. The synergism between gemini and these chemicals reduces the corrosion rate of N80 and increases the inhibition efficiency remarkably. All the mixture inhibitors are anodic type in nature. The inhibition action is exerted by inhibiting the anode process of corrosion.

#### ACKNOWLEDGEMENTS

We are grateful to the supports of National Science Foundation of China (No. 51641108) and the Sichuan Key Lab of Oilfield Materials (No. X151516KCL42).

#### References

1. E. A. Flores, O. Olivares, N. V. Likhanova, M. A. Domínguez-Aguilar, N. Nava, D. Guzman-Lucero, M. Corrales, *Corros. Sci.* 53 (2011) 3899.
2. M. A. Quraishi, I. Ahamad, A. K. Singh, S. K. Shukla, V. Singh, *Mater. Chem. Phys.* 112 (2008) 1035.
3. H. Wang, Y. Liu, J. Xie, J. Tang, M. Duan, Y. Wang, M. Chamas, *Int. J. Electrochem. Sci.* 11 (2016) 4943.
4. L. J. Mu, W. Z. Zhao, *Corros. Sci.* 52 (2010) 82.
5. K. G. Zhang, B. Xu, W. Z. Yang, X. S. Yin, Y. Liu, Y. Z. Chen, *Corros. Sci.* 90 (2015) 284.
6. L. Zhang, Y. He, Y. Q. Zhou, R. R. Yang, Q. B. Yang, D. Y. Qing, Q. H. Niu, *Petroleum* 1 (2015) 237.
7. S. Salimi, M. Nasr-Esfahani, S. A. Umoren, E. Saebnoori, *J. Mater. Eng. Perform.* 24 (2015) 4696.
8. J. Porcayo-Calderon, L. M. Martínez de la Escalera, J. Canto, M. Casales-Diaz, *Int. J. Electrochem. Sci.* 10 (2015) 3160.
9. M. A. Deyab, M. T. Zaky, M. I. Nessim, *J. of Mol. Liq.* 229 (2017) 396.
10. Y. Zuo, L. Yang, Y. Tan, Y. Wang, J. Zhao, *Corros. Sci.* 120 (2017) 99.
11. J. Zhao, G. Chen, *Electrochim. Acta* 69 (2012) 247.
12. P. C. Okafor, C. B. Liu, X. Liu, Y. G. Zheng, F. Wang, C. Y. Liu, F. Wang, *J. Solid State Electrochem.* 14 (2010) 1367.
13. S. Q. Hu, A. L. Guo, Y. F. Geng, X. L. Jia, S. Q. Sun, J. Zhang, *Mater. Chem. Phys.* 134 (2012) 54.
14. M. Heydari, M. Javidi, *Corros. Sci.* 61 (2012) 148.
15. J. Zhang, X. L. Gong, H. H. Yu, M. Du, *Corros. Sci.* 53 (2011) 3324.
16. P. C. Okafor, Y. G. Zheng, *Corros. Sci.* 51 (2009) 850.
17. P. C. Okafor, C. B. Liu, X. Liu, and Y. G. Zheng, *J. Appl. Electrochem.* 39 (2009) 2535.
18. F. E. Heakal, A. E. Elkholy, *J. Mol. Liq.* 230 (2017) 395.
19. D. Asefi, M. Arami, N. M. Mahmoodi, *Corros. Sci.* 52 (2010) 794.
20. M. A. Hegazy, M. Abdallah, H. Ahmed, *Corros. Sci.* 52 (2010) 2897.
21. J. M. Zhao, H. B. Duan, R. J. Jiang, *Corros. Sci.* 91 (2015) 108.
22. M. A. Hegazy, *Corros. Sci.* 51 (2009) 2610.
23. L. G. Qiu, A. J. Xie, Y. H. Shen, *Corros. Sci.* 47 (2005) 273.
24. C. Verma, E. E. Ebenso, M. A. Quraishi, *J. Mol. Liq.* 233 (2017) 403.
25. N. Anusuya, J. Saranya, P. Sounthari, A. Zarrouk, S. Chitra, *J. Mol. Liq.* 225 (2017) 406.
26. K. K. Anupama, K. Ramya, K. M. Shainy, A. Joseph, *Mater. Phys. Chem.* 167(2015) 28.

27. A. S. Fouda, M. A. Ismail, G. Y. Elewady, A. S. Abousalem, *J. Mol. Liq.* 240 (2017) 372.
28. J.A. Calderón, F.A. Vásquez, J.A. Carreño, *Mater. Phys. Chem.* 185 (2017) 218.
29. S. Vishwanatham, N. Haldar, *Corros. Sci.* 50 (2008) 2999.
30. M. V. Fiori-Bimbi, P. E. Alvarez, H. Vaca, C. A. Gervasi, *Corros. Sci.*, 92, (2015) 192.
31. Y. Hao, L. A. Sani, T. Ge, Q. Fang, *Corros. Sci.* 123 (2017) 158.
32. M. Yadav, Debasis Behera, Usha Sharma, *Arab. J. Chem.* 9 (2016) S1487
33. E. S. Ferreira, C. Giancomelli, F. C. Giacomelli, A. Spinelli, *Mater. Chem. Phys.* 83 (2004) 129.
34. L. G. Qiu, A. J. Xie, Y. H. Shen, *Appl. Surf. Sci.* 246 (2005) 1.
35. N. Yilmaz, A. Fitoz, ý. Ergun, K. C. Emregül, *Corros. Sci.* 111(2016) 110.
36. X. H. Li, S. D. Deng, G. N. Mu, H. Fu, F. Z. Yang, *Corros. Sci.* 50 (2008) 420.
37. H. H. Zhang, X. L. Pang, M. Zhou, C. Liu, L. Wei, K. W. Gao, *Appl. Surf. Sci.* 356 (2015) 63.
38. J. Cruz, R. Martínez , J. Genesca, E. García-Ochoa, *J. Electroanal. Chem.* 566 (2004) 111.
39. J. Haque, K. R. Ansari, V. Srivastava, M. A. Quraishi, I. B. Obot, *J. Ind. Eng. Chem.* 49 (2017) 176.
40. Mohammad Mobin, Saman Zehra, Mosarrat Parveen, *J. Mol. Liq.* 216 (2016) 598.
41. M. A. Hegazy, I. Aiad, *J. Ind. Eng. Chem.* 31 (2015) 91.
42. M. P. Desimone, G. Grundmeier, G. Gordillo, S. N. Simison, *Electrochim. Acta* 56 (2011) 2990.

© 2017 The Authors. Published by ESG ([www.electrochemsci.org](http://www.electrochemsci.org)). This article is an open access article distributed under the terms and conditions of the Creative Commons Attribution license (<http://creativecommons.org/licenses/by/4.0/>).